Reduced and Superreduced Diplatinum Complexes

Tania V. Darnton,[a,‡] Bryan M. Hunter,[a,‡] Michael G. Hill,[b] Stanislav Záliš,*[,c] Antonín Vlček Jr.,*[,c,d] and Harry B. Gray*[,a]

[a]Beckman Institute, California Institute of Technology, Pasadena, CA 91125, United States
[b]Occidental College, Los Angeles, California 90041, United States
[c]J. Heyrovský Institute of Physical Chemistry, Czech Academy of Sciences, Dolejškova 3, CZ-182 23 Prague, Czech Republic
[d]Queen Mary University of London, School of Biological and Chemical Sciences, Mile End Road, London E1 4NS, United Kingdom

‡ Indicates that these authors contributed equally.

SUPPLEMENTARY INFORMATION

FIGURES

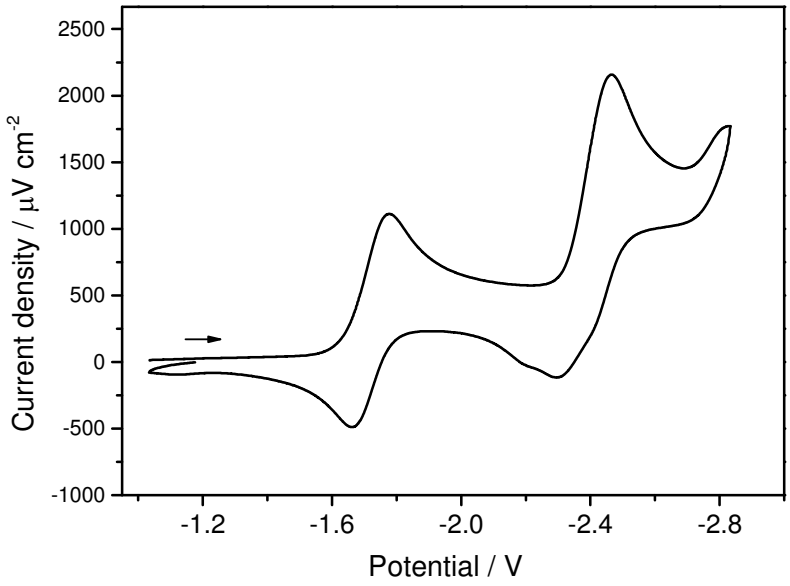

Figure S1. Cyclic voltammogram of $Pt(pop\text{-}BF_2)^{4-}$ in MeCN containing 0.1 M Bu_4NPF_6 at room temperature (~294 K). Potentials vs. Fc^+/Fc. Scan rate 50 mV/s.

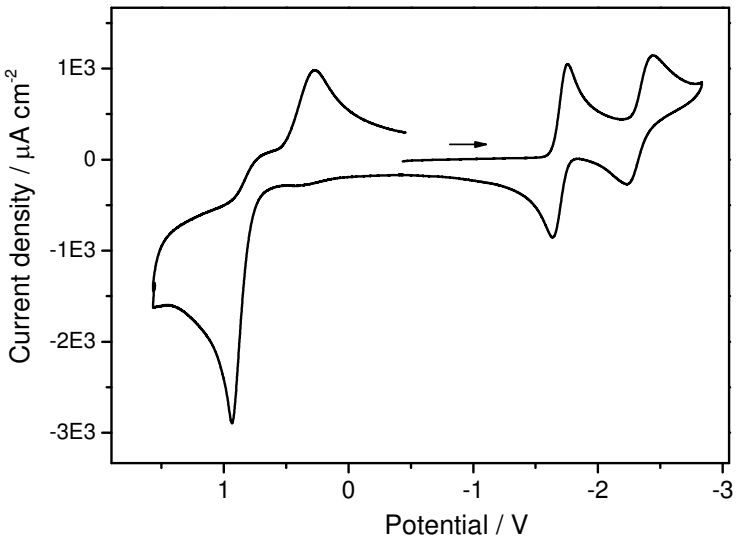

Figure S2. Full-range cyclic voltammogram of $Pt(pop\text{-}BF_2)^{4-}$ in MeCN containing 0.1 M Bu_4NPF_6 at 273 K. Potentials vs. Fc^+/Fc. Scan rate 200 mV/s.

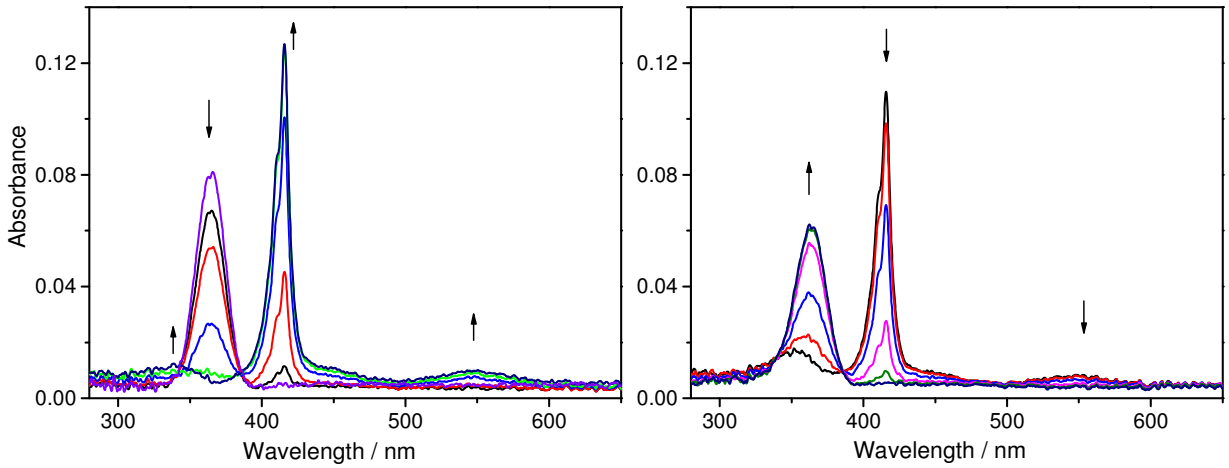

Figure S3. UV-vis absorption spectra monitored in the course of the first $Pt(pop\text{-}BF_2)^{4-}$ reduction to $Pt(pop\text{-}BF_2)^{5-}$ (left) and subsequent product reoxidation (right). The slightly lower intensities in the right panel are caused by product diffusion out of the spectroscopically probed region.

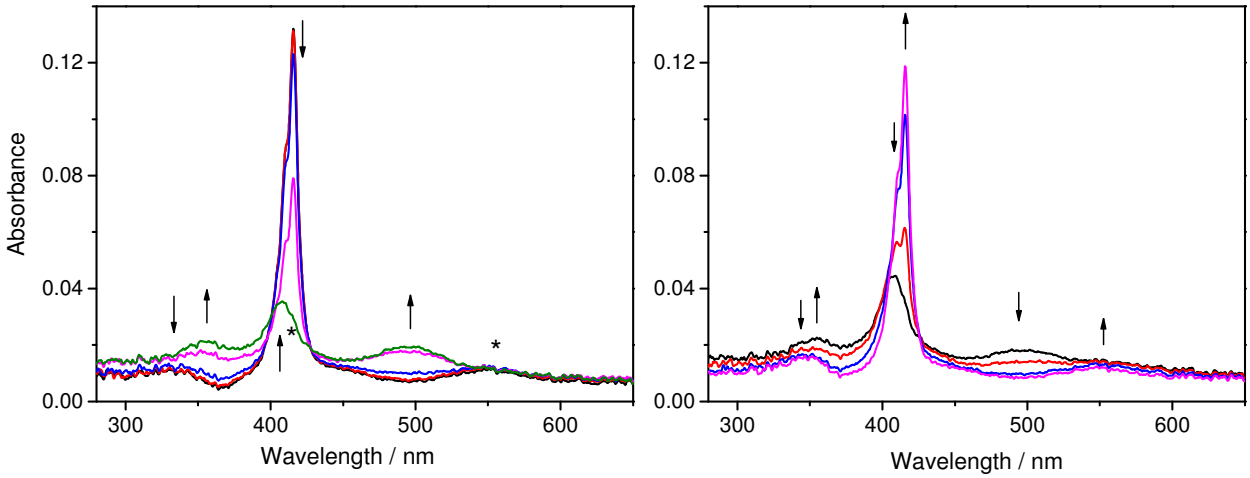

Figure S4. UV-vis absorption spectra monitored in the course of the second $Pt(pop\text{-}BF_2)^{4-}$ reduction (left) and subsequent product reoxidation (right). The slightly lower intensities in the right panel are caused by product diffusion out of the spectroscopically probed region.

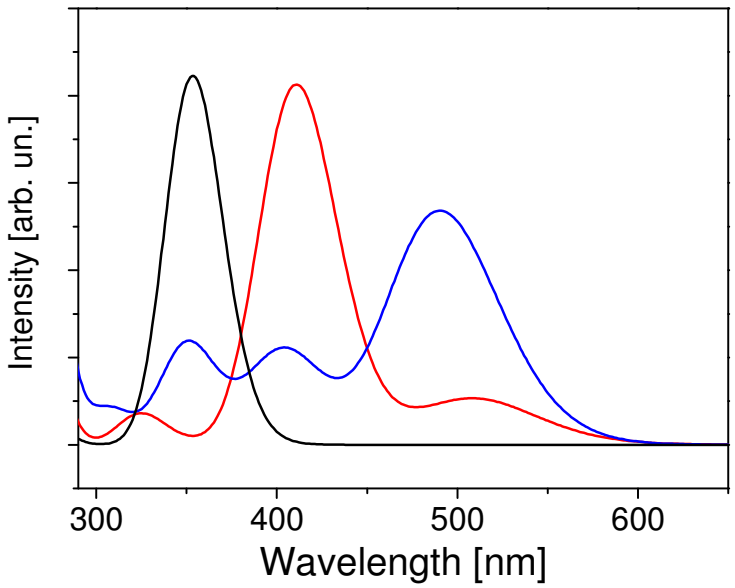

Figure S5a. TD-DFT simulated UV-vis absorption spectra of $Pt(pop\text{-}BF_2)^{n-}$ (n = 4 (black), 5 (red) and 6/conformer **6** (blue)). The same FWHM of 3000 cm^{-1} was assumed for all transitions. TD-DFT (PBE0/PCM-MeCN)

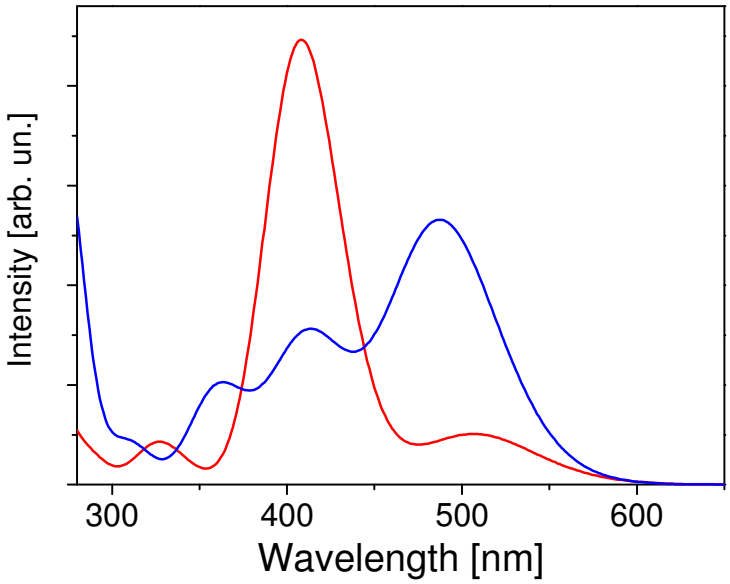

Figure S5b. TD-DFT simulated UV-vis absorption spectra of $Pt(pop\text{-}BF_2)^{n-}\cdot nMe_4N^+$ (n = 5 (red), 6/conformer **6** (blue)). The same FWHM of 3000 cm^{-1} was assumed for all transitions. TD-DFT (PBE0/PCM-MeCN)

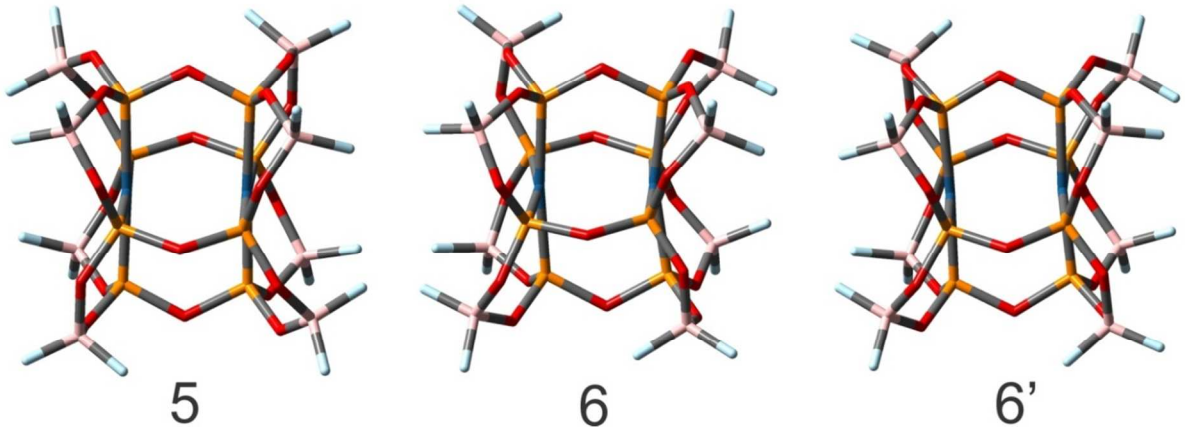

Figure S6. Left and middle: DFT-optimized structures of $Pt(pop\text{-}BF_2)^{5-}$ (**5**) and the **6** and **6'** conformers of $Pt(pop\text{-}BF_2)^{6-}$ in MeCN.

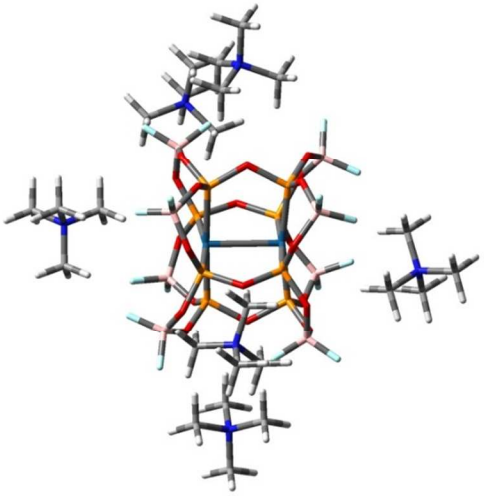

Figure S7. DFT-optimized structure of $Pt(pop\text{-}BF_2)^{6-}\cdot 6Me_4N^+$ in MeCN.

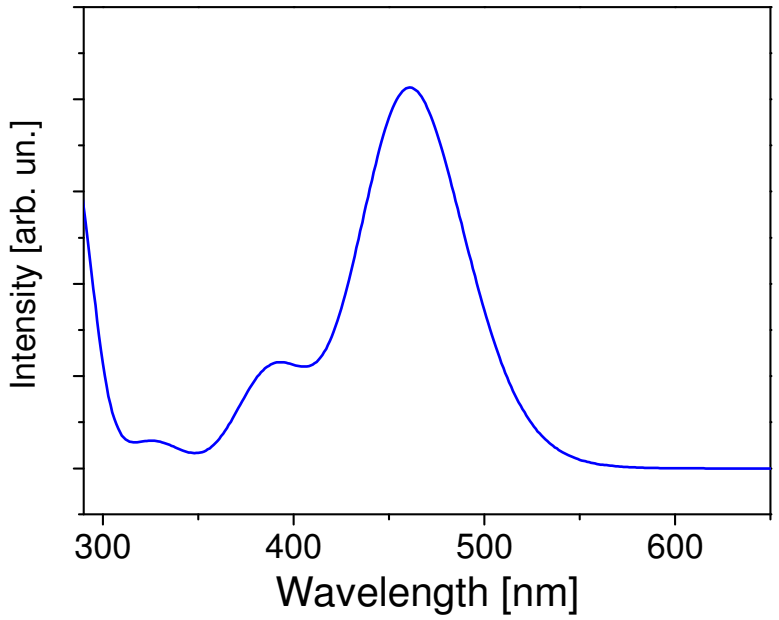

Figure S8. Calculated absorption spectrum of Pt(pop-BF_2)$^{6-}$, conformer **6'**. TD-DFT (PBE0/PCM-MeCN)

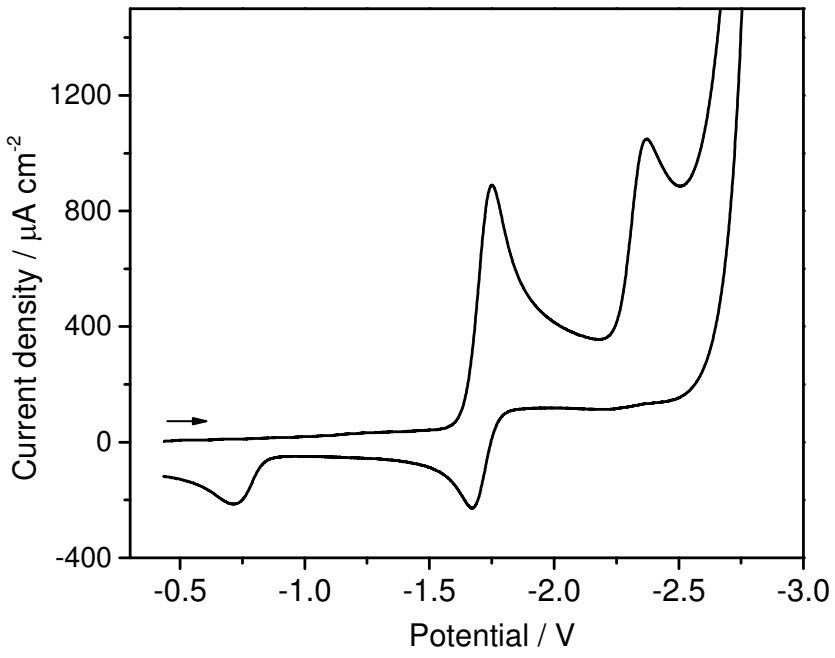

Figure S9. Cyclic voltammogram of Pt(pop-BF_2)$^{4-}$ in MeCN containing 0.1 M Bu_4NPF_6 and 1 mM CH_2Cl_2 at 273 K. Potentials vs. Fc^+/Fc. Scan rate 100 mV/s.

TABLES

Table S1. DFT (ADF/PBE0/COSMO-MeCN) calculated spin densities ρ and g and A(Pt) (in MHz) EPR parameters for $Pt(pop\text{-}BF_2)^{5-}$.

	calc.	exp.
ρ Pt (total)	0.552	-
ρ P (total)	0.389	-
g_1	1.987	1.98
g_2	2.035	2.03
g_3	2.047	2.04
g_1-g_3	0.060	0.060
g_{iso}	2.023[a]	
A_1(Pt)	599	900
A_2(Pt)	-430	550
A_3(Pt)	-428	550
A_1(Pt')	623	900
A_2(Pt')	-419	500
A_3(Pt')	-420	350

[a] Calculated as $g_{iso} = ((g_1^2 + g_2^2 + g_3^2)/3)^{1/2}$.

Table S2. DFT-calculated (PBE0/PCM-MeCN) structural parameters of $Pt(pop\text{-}BF_2)^{5-}$ and the two conformers of $Pt(pop\text{-}BF_2)^{6-}$. Atom P5 is in alignment with atom P1, etc.

Bond	n = 5	n = 6/conf **6**	n = 6/conf **6'**
Pt1-Pt2	2.803	2.739	2.745
Pt-P1	2.277	2.268	2.255
Pt-P2	2.277	2.258	2.255
Pt-P3	2.278	2.265	2.257
Pt-P4	2.278	2.255	2.257
Pt-P5	2.277	2.256	2.256
Pt-P6	2.277	2.260	2.255
Pt-P7	2.278	2.260	2.255
Pt-P8	2.278	2.266	2.256
P-O(-P) (average)	1.634	1.644	1.645
angle			
Pt2-Pt1-P1	91.9	87.3	93.1
Pt2-Pt1-P2	91.9	96.2	91.7
Pt2-Pt1-P3	90.8	87.5	91.7
Pt2-Pt1-P4	90.8	96.3	93.1
Pt2-Pt1-P5	91.9	97.1	92.3
Pt2-Pt1-P6	91.9	88.4	92.3
Pt2-Pt1-P7	90.8	96.8	90.8
Pt2-Pt1-P8	90.8	88.3	90.8

Table S3. TD-DFT (PBE0/PCM-MeCN) calculated lowest singlet excitation energies (eV) for $Pt(pop\text{-}BF_2)^{6-}$/ conformer **6'** with oscillator strength larger than 0.003.

State	Main contributing excitations (%)	Transition energy eV (nm)	Oscillator strength	Exptl. eV (nm)
b^1A	95 (HOMO $\rightarrow$ LUMO)	2.69 (461)	0.284	461
c^1A	93 (HOMO $\rightarrow$ LUMO+4)	3.18 (404)	0.076	490
d^1A	99 (HOMO $\rightarrow$ LUMO+6)	3.75 (331)	0.009	356
e^1A	98 (HOMO $\rightarrow$ LUMO+7)	3.84 (323)	0.012	